



# Predicting and testing continental vertical motion histories since the Paleozoic

Nan Zhang <sup>a,\*</sup>, Shijie Zhong <sup>a</sup>, Rebecca M. Flowers <sup>b</sup>

<sup>a</sup> Department of Physics, University of Colorado, Boulder, CO, USA

<sup>b</sup> Department of Geological Sciences, University of Colorado, Boulder, CO, USA

## ARTICLE INFO

### Article history:

Received 27 May 2011

Received in revised form 5 October 2011

Accepted 31 October 2011

Available online 5 December 2011

Editor: Y. Ricard

### Keywords:

mantle convection  
dynamic topography  
continental vertical motion  
thermochronology

## ABSTRACT

Dynamic topography at the Earth's surface caused by mantle convection can affect a range of geophysical and geological observations including bathymetry, sea-level change, continental flooding, sedimentation and erosion. These observations provide important constraints on and test of mantle dynamic models. Based on global mantle convection models coupled with the surface plate motion history, we compute dynamic topography and its history for the last 400 Ma associated with Pangea assembly and breakup, with particular focus on cratonic regions. We propose that burial-unroofing histories of cratons inferred from thermochronology data can be used as a new diagnostic to test dynamic topography and mantle dynamic models. Our models show that there are currently two broad dynamic topography highs in the Pacific and Africa for the present-day Earth that are associated with the broad, warm structures (i.e., superplumes) in the deep mantle, consistent with previous proposals of dynamical support for the Pacific and African superswells. Our models reveal that Pangea assembly and breakup, by affecting subduction and mantle upwelling processes, have significant effects on continental vertical motions. Our models predict that the Slave craton in North America subsides before Pangea assembly at 330 Ma but uplifts significantly from 330 Ma to 240 Ma in response to pre-Pangea subduction and post-assembly mantle warming. The Kaapvaal craton of Africa is predicted to undergo uplift from ~180 Ma to 90 Ma after Pangea breakup, but its dynamic topography remains stable for the last 90 Ma. The predicted histories of elevation change for the Slave and Kaapvaal cratons compare well with the burial-unroofing histories inferred from the thermochronology studies, thus supporting our dynamic models including the development of the African superplume mantle structure. The vertical motion histories for other cratons can provide further tests of and constraints on our mantle dynamic models.

Published by Elsevier B.V.

## 1. Introduction

Dynamic topography is the surface deflection induced by mantle convection driven by sub-lithospheric buoyancy forces and it may provide important constraints on mantle dynamic processes (e.g., Cazenave et al., 1989; Hager and Richards, 1989; Ricard et al., 1993). Inferring dynamic topography is often not straightforward, however, because the observed topography is sensitive to crustal and lithospheric structures that are commonly not well constrained especially in continents and tectonically active regions including plate boundaries. On the seafloor where crustal and lithospheric structures are relatively uniform and simple, residual or dynamic topography has been constructed by removing crustal and lithospheric contributions (e.g., Conrad et al., 2004; Davies and Pribac, 1993). Another approach in inferring dynamic topography considers the transient nature of dynamic topography and seeks constraints from the vertical motion history of continents (e.g., Gurnis, 1993; Mitrova et al., 1989) or oceanic islands (e.g., Zhong and Watts, 2002). In this approach, the elevation change of tectonically stable regions as

recorded by the history of continental flooding and deposition of sedimentary strata, provides constraints on the dynamic topography history.

There have been a large number of studies in the last 20 yr on dynamic topography and its history on both global and regional scales. The present-day dynamic topography was constructed through removing crustal and lithospheric effects (Cazenave et al., 1989; Davies and Pribac, 1993; Panasyuk and Hager, 2000). Lithgow-Bertelloni and Silver (1998), using mantle dynamic models, proposed that the anomalous elevations of southern Africa are supported by the African superplume. Gurnis et al. (1998), Mitrova et al. (1989), Pysklywec and Mitrova (1999), and investigated the role of subducted slabs in producing the continental subsidence and stratigraphic records in the western US, South Africa, and Australia, respectively. Gurnis (1993) studied the effects of subducted slabs on continental flooding in the Phanerozoic using the locations of subduction zones in paleogeography reconstruction models. Lithgow-Bertelloni and Gurnis (1997) discussed the effects of slab-induced dynamic topography on global continental vertical motions in the Cenozoic. Dynamic topography histories for the last tens of Ma were also reconstructed for North America, South America and Africa using seismic and mantle flow constraints (Liu et al., 2008; Moucha and Forte, 2011; Moucha et al., 2008; Spasojević et al., 2009; Shephard et al., 2010).

\* Corresponding author. Present address: Department of Geological Science, Brown University, RI, USA.

E-mail address: [nan.zhang@colorado.edu](mailto:nan.zhang@colorado.edu) (N. Zhang).

The key to reconstructing the history of dynamic topography is to reproduce the time evolution of mantle buoyancy structures. Although mantle convection models using plate motion histories have been formulated to constrain mantle structure evolution (e.g., Bull et al., 2009; Bunge et al., 1998; McNamara and Zhong, 2005) and surface vertical motion histories (e.g., Moucha et al., 2008), no mantle structures and hence vertical motion histories have been reconstructed back into the Paleozoic. One difficulty in reconstructing the pre-Cretaceous mantle structure history is the lack of constraints on the plate motion history for the Paleo-Pacific Ocean before 120 Ma (e.g., Lithgow-Bertelloni and Richards, 1998; Ricard et al., 1993), although continental plate motions in the African hemisphere since the Paleozoic are well constrained and the history of Pangea assembly and breakup is relatively well understood (e.g., Scotese, 2001). In a recent study (Zhang et al., 2010), we constructed a proxy global plate motion for the last 450 Ma to examine the effects of Pangea on mantle structure evolution. Our model, while reproducing present-day degree-2 mantle structures (i.e., the African and Pacific superplumes and circum-Pacific subduction structures), shows that the African superplume may not have developed until ~200 Ma (Zhang et al., 2010). Recently, we reconstructed the temporal and spatial variations of heat flux at the Earth's surface and CMB for the last 400 Ma based on this convection model (Zhang and Zhong, 2011). However, the timing of African superplume formation is debated; for example, Torsvik et al. (2010) suggest that the African superplume has been stable for as long as ~500 Ma.

The main goals of this study are 1) to construct a model for global dynamic topography and continental vertical motion histories since Paleozoic time using mantle convection models coupled with the plate motion history (Zhang et al., 2010) and 2) to evaluate the feasibility of our results by comparing the predicted vertical motion histories with geological constraints on the history of elevation change for four Archean cratonic regions in North America, South Africa, South America, and Australia. Cratons by definition have been relatively stable and unaffected by major orogenesis typically for hundreds of millions of years, and thus are especially useful for this analysis. Distinct from previous work, our study represents the first effort to reconstruct global dynamic topography from a time-dependent convection model in which heat transfer and thermal and buoyancy structures are dynamically determined. We are particularly interested in understanding how the assembly and breakup of Pangea influence continental vertical motions, how the vertical motions compare with those inferred recently for two of these cratons from thermochronology studies (Ault et al., 2009; Flowers and Schoene, 2010; Flowers et al., submitted for publication), and how these vertical motion histories may help constrain mantle dynamics including the evolution of the African superplume. This paper is organized as follows. Section 2 describes model setups and the method for computing the dynamic topography. Section 3 presents model results for dynamic topography. Comparison of our model results with the present day dynamic topography and cratonic vertical motion histories are discussed in Section 4, with the conclusions presented in the final section.

## 2. Models and methods

Our global models of mantle convection with the last 450 Ma plate motion history are the same as that described in Zhang et al. (2010). Here we only describe the basic model set-ups and calculations of dynamic topography. Our models assume an infinite Prandtl number and the Boussinesq approximation. The conservation equations of mass, momentum, and energy, and the advection equation of compositions are described in Zhong et al. (2008). Our mantle convection models have four important parameters: internal heat generation rate  $H$ , buoyancy number  $B$ , Rayleigh number  $Ra$ , and temperature- and depth-dependent viscosity  $\eta$ , as defined and described in Zhang et al. (2010).

Mantle viscosity is given by  $\eta = \eta_0(r) \exp[E(0.5 - T)]$ , where  $\eta_0(r)$  is the depth-dependent pre-factor, and  $T$  and  $E$  are the non-dimensional

temperature and activation energy, respectively. The depth-dependent pre-factor  $\eta_0(r)$  for mantle viscosity are 1 and 1/30 for the 150 km thick lithosphere and the upper mantle, respectively, and for the lower mantle,  $\eta_0(r)$  increases linearly from 2.0 at the 670 km depth to 6.8 at the CMB (Zhang et al., 2010). This leads to a mantle viscosity structure in which the lower mantle is ~2 orders of magnitude more viscous than the upper mantle.  $E$  is 9.21 in this study, giving rise to viscosity variations of  $10^4$  due to temperature variations. This activation energy  $E$ , if scaled using parameters in Table 1, is about half of that determined from laboratory studies for olivine (e.g., Karato and Jung, 2003). However, the use of reduced  $E$  in convection models with Newtonian rheology such as ours is supported by both numerical experiments (e.g., Christensen, 1984) and also modeling in-situ observations (e.g., van Hunen et al., 2005).

Our global plate motion model for the last 450 Ma consists of 34 different stages and was fully described in Zhang et al. (2010). Our plate motion model for the last 120 Ma uses the published model by Lithgow-Bertelloni and Richards (1998) and Ricard et al. (1993). For plate motions before 120 Ma, our model considers realistic continental plate motions in the African hemisphere (Scotese, 2001), but plate motions in the Pacific hemisphere are assumed to resemble those at 120 Ma.

The model calculations are performed with CitcomS (Zhong et al., 2008). Isothermal boundary conditions are applied at the surface with non-dimensional temperature 0.0 and CMB with temperature 1.0 in all calculations. We use a grid with ~3,150,000 elements (i.e.,  $12 \times 64^3$  elements, see Zhong et al., 2000) for all the cases in this study. The top and bottom boundary layers use a refined grid with 15 km and 23 km vertical resolution, respectively.

Our modeling has two steps. First, we determine the evolution of the thermochemical structures (i.e., the buoyancy structures) of the mantle using the time dependent mantle convection model coupled with plate motion history (Zhang et al., 2010). All the cases start with one-dimensional initial temperature profiles derived from pre-calculations that use the same model parameters except that the plate motion boundary condition is replaced with a free-slip boundary condition. For most models, surface plate motions for the first stage (i.e., at 450 Ma ago) are employed for 150 Ma before the plate motions are updated with subsequent plate motion history (Zhang et al., 2010), but the duration of the initial run is also varied to study its effect on the mantle structures. Consequently, only model mantle structures and hence the dynamic topography for the last ~400 Ma are interpreted in this study. Second, for the time period of interest, we compute dynamic topography by re-solving the Stokes' flow problem using the mantle buoyancy from our first step calculation. We also replace the plate motion boundary condition with free-slip boundary condition and reduce lithospheric viscosity (Davies, 1989; Ghosh et al., 2010; Zhong and Davies, 1999). We reduce the lithospheric viscosity so that the averaged surface horizontal velocity is similar to the imposed plate motion. However, the lithospheric viscosity is also varied to check for its effect on dynamic topography. Self-gravitation is not included in our calculations of dynamic topography, which may introduce ~15% amplitude difference at very long-wavelengths (e.g., Zhong et al., 2008). The parameters for scaling the stress and dynamic topography are also shown at Table 1.

**Table 1**  
Model parameters and material properties.

Parameters	Value
Earth's radius, $R$	6370 km
CMB radius	3503.5 km
Gravitational acceleration, $g$	$9.8 \text{ m.s}^{-2}$
Thermal diffusivity, $\kappa$	$10^{-6} \text{ m}^2.\text{s}^{-1}$
Coefficient of thermal expansion, $\alpha$	$2 \times 10^{-5} \text{ K}^{-1}$
Temperature difference, $\Delta T$	2500 K
Mantle density, $\rho$	$3300 \text{ kg.m}^{-3}$

### 3. Results

In this section, we first demonstrate the role of lithospheric and mantle buoyancy in topography, thus defining dynamic topography for this study. Second, we present the results of dynamic topography and its history for the reference case TG1. We then examine the effects of different parameters including chemical piles, initial mantle structures, and plate geometry of the oceanic plates on dynamic topography.

#### 3.1. The model present-day topography and dynamic topography from case TG1

We start with the reference case TG1 that is the same as case HF1 in Zhang and Zhong (2011) or case FS1 in Zhang et al. (2010). This case has an initially 250 km thick chemical layer above the CMB with a buoyancy number  $B$  of 0.5. With  $Ra = 2 \times 10^8$  and other parameters listed in

Table 1, the averaged viscosities for the upper mantle and lower mantle are  $\sim 4.5 \times 10^{19}$  Pa s and  $\sim 7 \times 10^{21}$  Pa s, respectively. Internal heat generation rate  $H$  is 100, which yields 62% internal heating ratio, implying a significant fraction of heating from the core (e.g., Leng and Zhong, 2008). This case reproduces well the present-day seafloor age and heat flux distributions (Zhang and Zhong, 2011) and long-wavelength mantle structures (Zhang et al., 2010). Given that seafloor topography and heat flux are both mainly controlled by lithospheric thermal structure or seafloor age (e.g., Parsons and Sclater, 1977), we expect that the total topography on the seafloor from our model including mantle and lithospheric buoyancy resembles the observed.

The model present-day topography is generally positive in oceanic regions, but broad negative model topography occurs in continental regions (Fig. 1A). This is because continental lithosphere is generally older and colder than oceanic lithosphere. Subduction zones show more localized, large negative topography, because of subducted

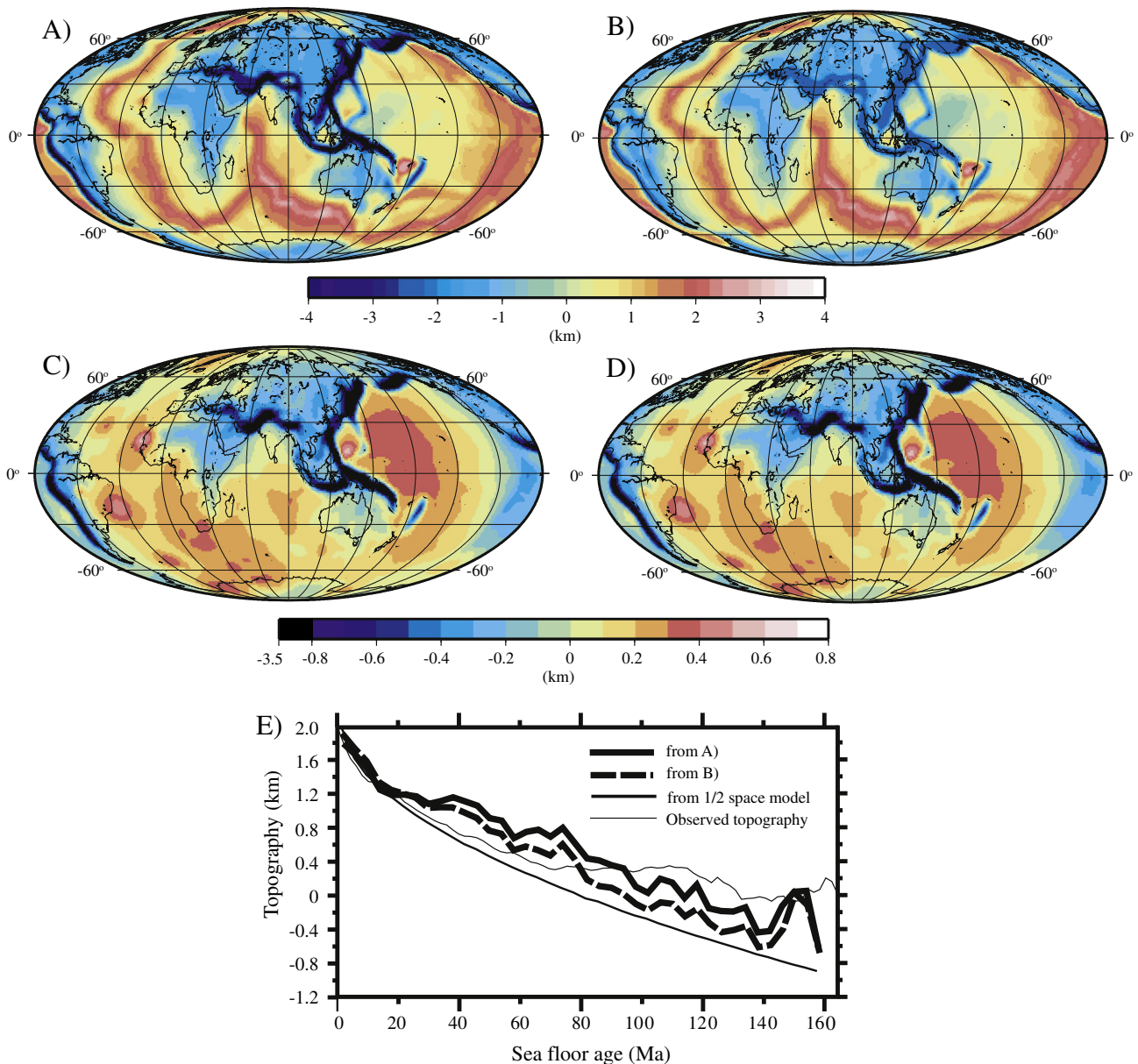


**Fig. 1.** The predicted present-day topographies using the whole mantle buoyancy (A) and the buoyancy within the top 200 km (B), the topography difference between A and B (C), the dynamic topography (i.e., using the mantle buoyancy below the 200 km depth) (D), and the topography–age relationships for the Pacific plate for the observed bathymetry, modeled topography, and that predicted from the half-space cooling model (E). In Fig. 1E, the observed bathymetry curve is from Zhong et al. (2007) in which surface topography anomalies associated with sediments, seamounts, and large igneous provinces are removed, and the model age distribution used for other curves is taken from Zhang and Zhong (2011). For the half-space cooling model, the topography  $w = 2\alpha T_m \sqrt{kt/\pi}$ , where  $T_m$  is the temperature at the upper mantle from the model and  $t$  is the seafloor age.

slabs. The lack of continental crust and realistic subduction zone processes in our model, however, prevents us from directly comparing them with the observed trench and continental topography. However, negative topography in continental regions in our model is generally consistent with the residual topography with removal of continental crust (Panasyuk and Hager, 2000).

The model topography (Fig. 1A) resembles the observed in oceanic regions outside oceanic trenches. For example, the topography is high at the mid-ocean ridges and decreases with distance from the ridges. Using the model seafloor age determined from Zhang and Zhong (2011), we plot averaged seafloor topography against seafloor age for the Pacific plate (Fig. 1E). The topography difference between the ridges and ~160 Ma old seafloor is ~2.5 km (Fig. 1A and E), comparable to the observed (note that our model topography ignores the ocean). We also compute the topography due to lithospheric cooling using the model seafloor age based on the half-space cooling model (e.g., Parsons and Sclater, 1977) (Fig. 1E). In plotting topography versus age, the topography is chosen to be the same as that from the mantle dynamic model at age of 20 Ma, because the model lithospheric thermal structure at mid-ocean ridges may not be as accurately resolved as for the relatively older plates. The topography from the half-space cooling model follows the same trend as that from our dynamic model but has larger amplitude (Fig. 1E). This is similar to how the observed seafloor topography compares with the half-space cooling model, and the difference is often called as residual or dynamic topography (e.g., Davies and Pribac, 1993).

The lithospheric thermal structure and buoyancy are largely responsible for the model topography in Fig. 1A. To demonstrate this, we compute model topography (Fig. 1B) using only the mantle and lithospheric buoyancy for the top 200 km but the same mantle viscosities. Notice that the top 200 km here includes the 150 km thick lithosphere and 50 km viscosity transition zone in our model. The resulting topography has similar patterns to that determined from the whole mantle buoyancy, but the amplitude is reduced. The topography–age relation for the Pacific from the model with only the top 200 km buoyancy (i.e., lithospheric buoyancy) is more similar to that for the half-space cooling model (Fig. 1E).

The difference between topographies in Fig. 1A and B, shown in Fig. 1C, reflects the contribution from the mantle buoyancy below 200 km depth, i.e., the dynamic topography. Generally, the dynamic topography is controlled by the large-scale mantle structures including cold downwellings and broad, warm upwellings that produce negative and positive dynamic topographies, respectively. Two major topography highs occur in the central Pacific and southwest Africa and its adjacent oceans (Figs. 1C and 2M). The Pacific dynamic topography high is on average ~400 m, occurring mostly for seafloor older than 60 Ma (Fig. 1C and E), while the African dynamic topography high is ~300 m. The Pacific dynamic topography high is responsible for the reduced topography at old seafloor relative to the half-space cooling model predictions (Fig. 1E). These two dynamic topography highs are related to the Pacific and African superplume structures (Fig. 2N). The dynamic topography can also be computed directly from mantle buoyancy below 200 km depth, as shown in Fig. 1D that is nearly identical to that in Fig. 1C. Therefore, for computing dynamic topography at different times, we will simply use mantle buoyancy below 200 km depth, as done in previous studies (Hager and Richards, 1989).

### 3.2. The dynamic topography history from case TG1

We first describe the general patterns of mantle buoyancy evolution that control dynamic topography history. There is no cold downwelling in the central Pacific in our model (Fig. 2 middle and right columns), while the distributions of the cold downwellings in the African hemisphere and circum-Pacific regions vary significantly with time, as a result of plate motion history (Zhang et al., 2010). During Pangea formation, a major mantle downwelling develops in the

African hemisphere as a result of convergence between Gondwana and Laurussia and this downwelling pushes the chemical piles towards the Pacific hemisphere (Fig. 2B). After Pangea formation and the cessation of convergence between Gondwana and Laurussia, the African hemisphere mantle warms up, and the circum-Pangea subduction pushes part of the hot chemical piles back to the African hemisphere (Fig. 2E) (Zhang et al., 2010). The opening of the Tethys Ocean after 290 Ma causes strong return flows in the mantle beneath eastern Laurussia (Fig. 2E). As Pangea starts to break up at 190 Ma, the subduction at southeast Pangea plays an important role in separating the African superplume from the Pacific superplume and sweeping the African superplume westward to eventually form the two superplume structures as imaged seismically for the present-day mantle (Fig. 2H, K, and N) (Zhang et al., 2010).

Dynamic topography is quantified from 400 Ma to the present day based on the time-dependent mantle structures (Fig. 2). Two distinct features in dynamic topography deserve some discussions before we present dynamic topography history. First, at 330 Ma, there is a broad, significant depression in Laurussia, particularly on its southwest part, i.e., now North America (Fig. 2A). This is related to the major downwelling below Laurussia that develops as Pangea forms (Fig. 2B). However, southern part of Pangea (i.e., Gondwana) shows mostly topography highs at this time, again reflecting the relatively warm mantle below. Since most continents belong to either Laurussia or Gondwana, the dynamic topography at this time is important for understanding the continental dynamic topography history to be presented later. Second, as a result of the assumed model plate motion history, the Pacific hemisphere is always dominated by major upwellings and broad topography highs. However, mid-ocean ridges are often associated with reduced dynamic topography, relative to older seafloor in the model (e.g., Fig. 2J and M). This reflects the fact that the spreading centers are passive, and that the warm mantle occurs below the old part of oceanic plates due to the mantle upwellings there and/or lithospheric insulation (Fig. 2O) (e.g., Huang and Zhong, 2005; King et al., 2002).

Now we describe the temporal–spatial variations of dynamic topography for continents. Generally, the formation of Pangea at 330 Ma leads to a large topography low in its northern part (i.e., North America, Europe, and Siberia) and a large topography high in its southern part (i.e., Africa, Antarctica, India, and Australia) (Fig. 2A). After the formation of Pangea, the cessation of subduction between Gondwana and Laurussia and warming up of the mantle below Laurussia lead to significant uplift of North America and Europe between 330 Ma and 250 Ma (Fig. 2D and G). Also, after 330 Ma, the circum-Pangea subduction and the Tethys subduction play an important role in causing topography lows in different continents, for example, in western North America (Fig. 2D, G, J, and M), western South America (Fig. 2D), and sometimes southern Africa (e.g., Fig. 2G). The subduction between the Paleo-Izanagi plate and Siberia and the Tethys subduction (Fig. 2D) cause a topography low in Siberia from 250 to 150 Ma. In contrast, the India and Australia continents maintain dynamic topography highs before 100 Ma because of their large distance from major subduction zones (Fig. 2D, G, and J), although they start to subside after their collision with the Eurasia and Pacific plates (Fig. 2M).

We choose four representative cratonic regions: the Slave craton, Kaapvaal craton, Sao Francisco craton, and Yilgarn craton from North America, South Africa, South America, and Australia, respectively, and track their time-dependent dynamic topographies (Fig. 2 for their locations at different times, and Fig. 3A). For each craton, we calculate the average dynamic topography over a circular region of 5° radius. It is clear that the Slave craton has been influenced by the major downwelling between Laurentia and Gondwana during Pangea assembly. After Pangea formation, the Slave craton is uplifted significantly, but the uplift of ~900 m is mostly completed at ~240 Ma (Fig. 3A). The subsequent vertical motion for the Slave craton is

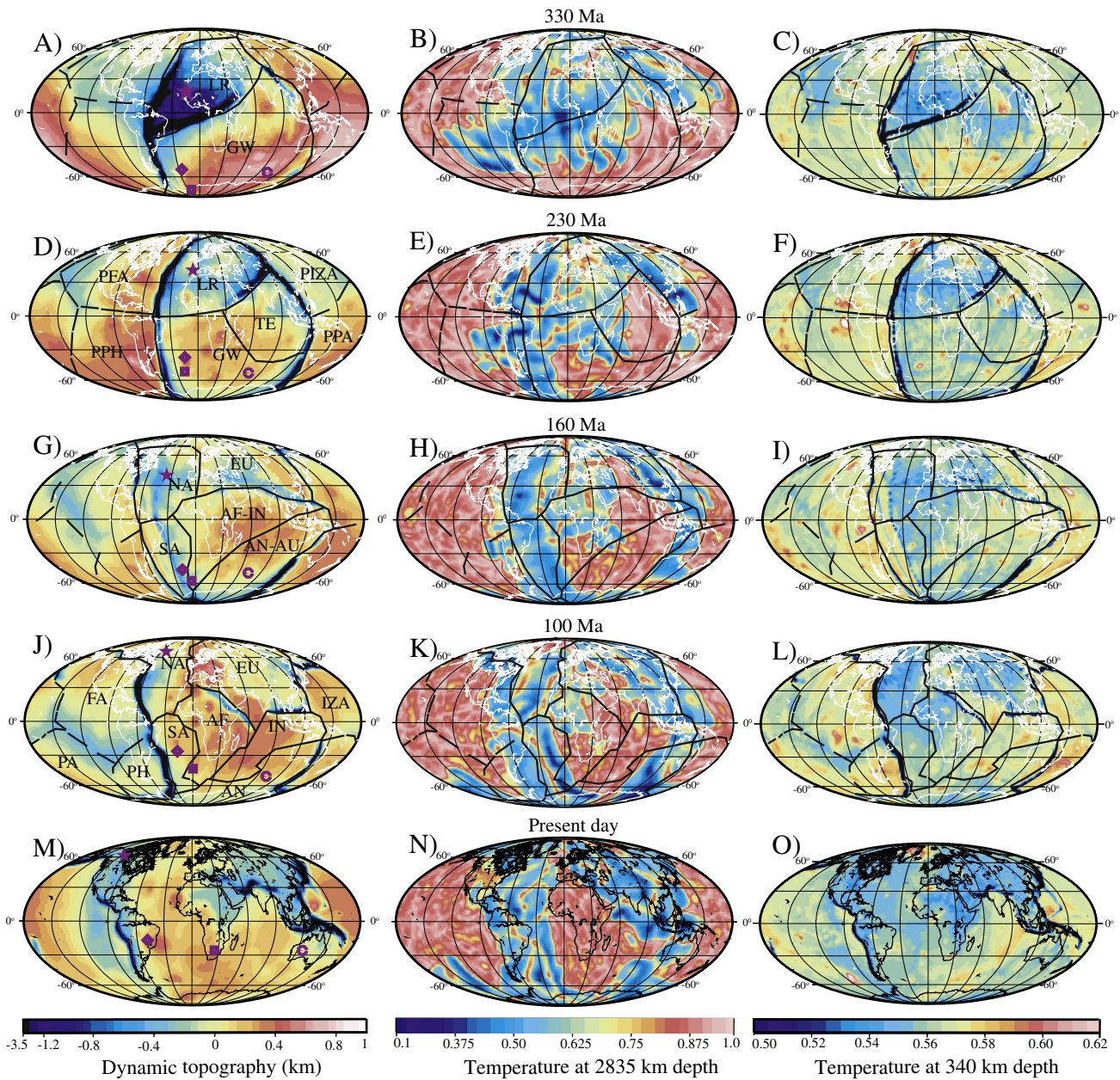


**Fig. 2.** The dynamic topographies (left column), mantle thermal structures at 2835 km depth (middle column), and at 340 km depth (right column) for time 330 Ma (A, B, and C), 230 Ma (D, E, and F), 160 Ma (G, H, and I), 100 Ma (J, K, and L), and the present day (M, N, and O) from case TG1. The star, square, diamond, and circle on the topography maps represent the locations of the Slave (112°W, 63°N), Kaapvaal (22°E, 25°S), Sao Francisco (45°W, 20°S), and Yilgarn (125°E, 25°S) cratons, respectively, with their present-day coordinates given in the parentheses. The abbreviations for tectonic plates are given in an alphabetic order as: AF for Africa, AN for Antarctica, AU for Australia, EU for Eurasia, FA for Farallon, GW for Gondwana, IN for India, IZA for Izanagi, LR for Laurasia, NA for North America, PA for Pacific, PFA for Paleo-Farallon, PH for Phoenix, PIZA for Paleo-Izanagi, PPA for Paleo-Pacific, PPH for Paleo-Phoenix, SA for South America, and TE for Tethys.

modest and is probably mostly affected by the subduction of the Farallon plate beneath North America (Fig. 2G, J, and M). As we will discuss later, some of temporal variations in dynamic topography in Fig. 3 are caused by small-scale features such as plumes (e.g., Fig. 2D and F) that are sensitive to model setups and cannot be reliably predicted. Therefore, it is important that we only interpret the robust model results.

The dynamic topography for the Kaapvaal craton decreases by ~500 m from 400 to 290 Ma with no clear relation to the assembly of Pangea (Fig. 3A). The dynamic topography increases modestly from 260 Ma to 220 Ma before dropping to the minimum at ~180 Ma. From 180 Ma to 90 Ma, following the breakup of Pangea, the dynamic topography at the Kaapvaal craton increases by ~500 m, and it remains stable for the last 90 Ma (Fig. 3A). As pointed

out earlier, the initially high dynamic topography of the Kaapvaal craton results from the relatively warm mantle below Gondwana (Fig. 2A–C). The subsequent variations of dynamic topography before 180 Ma depend on the distance of the Kaapvaal craton to the subduction zones (Fig. 2D) and other small-scale features such as plumes (e.g., Fig. 2F). The uplift from 180 Ma to 90 Ma arises as the craton moves away from subduction zones to the African superplume (Fig. 2G, J and M).

The Sao Francisco craton in South America shows similar temporal variations in dynamic topography to those for the Kaapvaal craton before 150 Ma because they are geographically close to each other before the opening of the South Atlantic Ocean. The Sao Francisco craton starts to separate from the Kaapvaal craton at 150 Ma, and moves over the African superplume, causing uplift from 150 and

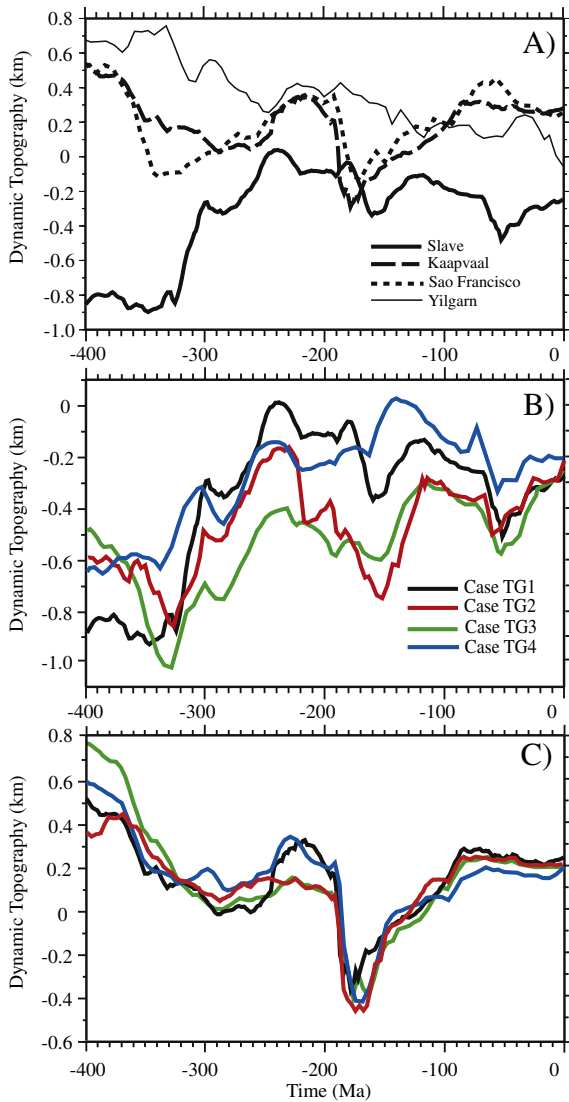


**Fig. 3.** The dynamic topography histories from case TG1 for the Slave, Kaapvaal, Sao Francisco, and Yilgarn cratons (A), and for Slave (B) and Kaapvaal (C) cratons from cases TG1, 2, 3, and 4.

60 Ma (Fig. 3A). The Sao Francisco craton shows ~250 m subsidence for the last 60 Ma, as it moves away from the African superplume (Fig. 2). The dynamic topography of the Yilgarn craton shows to first order a monotonic decrease for the last 400 Ma, differing from other three cratons (Figs. 2 and 3A). The Yilgarn craton is supported by the upwellings beneath southern Gondwana before Pangea formation (Fig. 2A). After Pangea formation, sitting on the east edge of Pangea, the Yilgarn craton subsides as the mantle below Pangea warms up to form the African superplume and to cause uplifts at the center of Pangea (Figs. 2D and 3). After Pangea breakup, the Yilgarn craton moves away from the African superplume and continues subsiding through the present day (Figs. 2G, J, M, and 3).

### 3.3. Influences of different parameters on the dynamic topography

We now present three more cases (cases TG2–TG4) in which we remove the chemical layer, vary the initial mantle structures, and change the plate geometry of the oceanic plates, to examine these effects on the dynamic topography. In comparing the vertical motion history for those four cratons, we will focus on the Slave and Kaapvaal cratons. This is because the Yilgarn craton in these cases shows

similar vertical motions to those in case TG1, while vertical motions of the Sao Francisco craton are similar to those for the Kaapvaal craton.

Case TG2 differs from case TG1 only by removing the chemical layer above the CMB (i.e., a purely thermal convection case). Case TG2 is the same as case HF2 in Zhang and Zhong (2011). With the removal of the chemical layer, mantle convection in case TG2 is more vigorous than in case TG1, and the internal heating ratio is 51%. The model present-day dynamic topography (Fig. 4J) and dynamic topography histories for those four cratons (Fig. 3B and C) show similarities to those from case TG1, although the amplitude of the dynamic topography from case TG2 appears larger. The smaller dynamic topography from case TG1 is expected because chemical boundaries in the mantle in case TG1 support convective stress and reduce dynamic topography (e.g., Hager and Richards, 1989; Le stunff and Ricard, 1997; Wen and Anderson, 1997). This suggests that the surface dynamic topography is insensitive to the chemical layer above the CMB. For example, the Slave craton shows similar uplift from 330 to ~240 Ma after Pangea formation (Fig. 3B), and the Kaapvaal craton displays similar uplift from 180 to 90 Ma (Fig. 3C). However, compared to case TG1, the Slave craton shows larger subsidence at ~150 Ma (Fig. 4G), while Kaapvaal craton has a larger subsidence at 180 Ma but no uplift between 260 and 200 Ma (Fig. 3C). The disappearance of the uplift between 260 and 200 Ma for the Kaapvaal craton in case TG2 arises because the plume that causes this uplift in case TG1 (Fig. 2D and F) is absent in case TG2 (Fig. 4D and F). As we will show later, the magnitude of uplift for the Slave craton at ~230 Ma also depends on whether small plumes exist close to the craton (Fig. 2D and F). This suggests that caution needs to be exercised in interpreting dynamic topography associated with localized plumes.

Case TG3 differs from case TG1 in that it has a 50 Ma initial run of the first stage plate motion instead of 150 Ma, and otherwise these two cases are identical. The temporal variations of dynamic topography for the four cratons from case TG3 remain similar to those from case TG1, particularly after 330 Ma (e.g., Fig. 3B and C). With a shorter initial run of the first stage plate motion, there is less subducted material in the mantle between Gondwana and Laurussia and the mantle beneath Laurussia is not as cold before 450 Ma, compared to case TG1. This leads to continuous cooling of the mantle beneath Laurussia from 450 to 330 Ma before the formation of Pangea, causing continuous subsidence in Laurussia and the Slave craton before 330 Ma (Fig. 3B). Case TG3 again suggests that dynamic topography associated with small thermal plumes is sensitive to model set-up and initial conditions. For example, the uplift of the Kaapvaal craton at ~220 Ma does not occur in case TG3 (Fig. 3C), although other features of the vertical motion history for the craton remain unchanged compared to case TG1. Likewise, the Slave craton uplift at ~240 Ma in case TG1 is more subdued in case TG3 (Fig. 3B) due to the absence of the small plume in case TG3 that exists in case TG1 (Fig. 2D and F).

Both of the subduction zones at western and southern margins of Laurussia during Pangea formation contribute to large subsidence of North America at ~330 Ma (Fig. 2A). However, there are some uncertainties about the nature of western plate boundary of North America during the Paleozoic and Mesozoic (Ward, 1995). In case TG4, we change the geometry and motion of the oceanic plates before 119 Ma to investigate the influence of an alternative position of the Paleo-Farallon plate on the dynamic topography for the Slave craton. In case TG4, the oceanic plate geometry and plate motions in the Pacific hemisphere before 119 Ma are rotated by 120°, compared with that used in case TG1, and cases TG4 and TG1 are otherwise identical. Case TG4 is the same as case HF11 in Zhang et al. (2010). This rotation of oceanic plates leads to the intersection of a ridge with North America ~40°–50° further north, or the Slave craton closer to a ridge, compared to case TG1 (Fig. 2D). As a result, the subducted slab below North America is younger and more buoyant, causing ~300 m less subsidence for the Slave craton at ~330 Ma (Fig. 3B). However, the

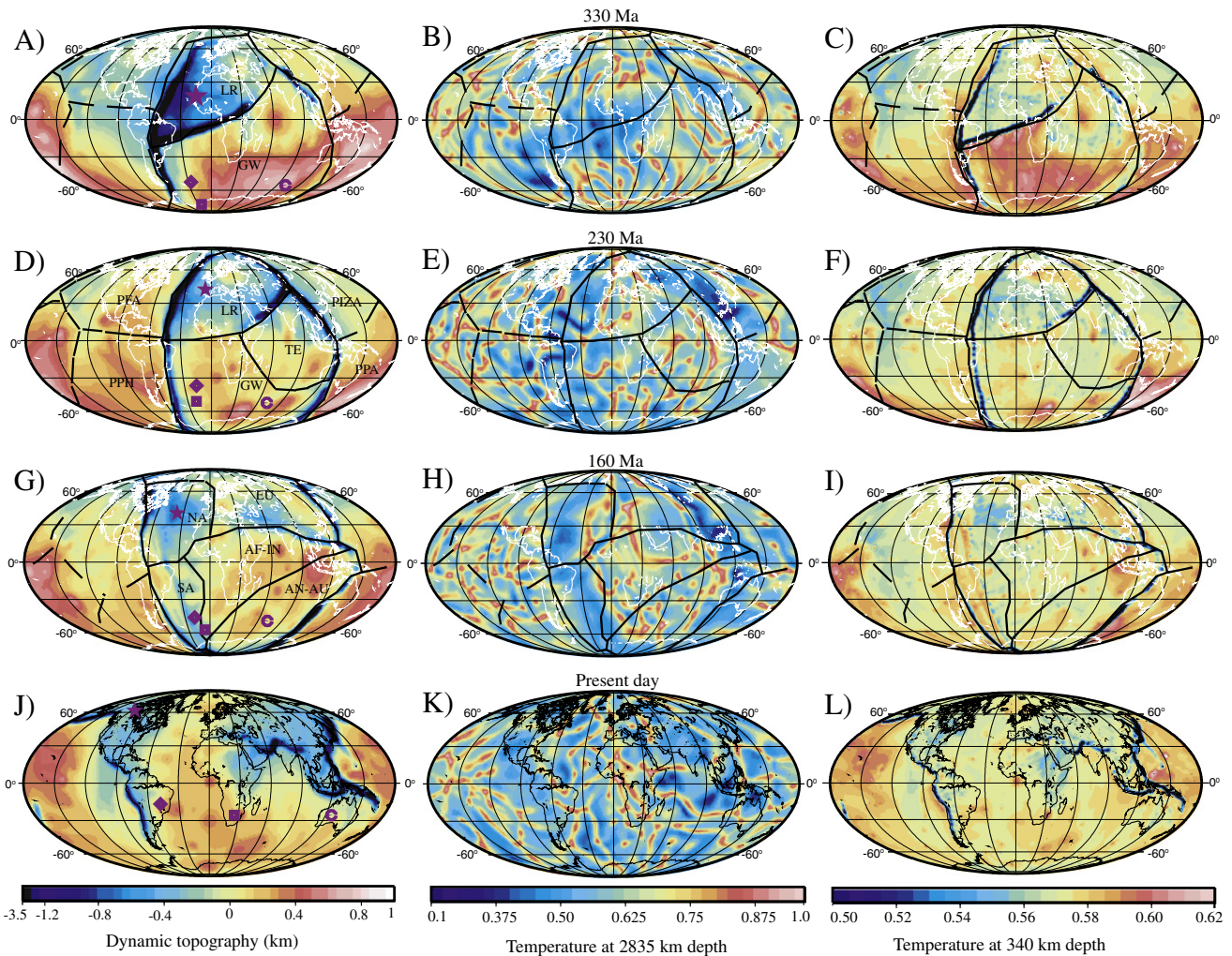


**Fig. 4.** The dynamic topographies (left column), mantle thermal structures at 2835 km depth (middle column), and at 340 km depth (right column) for time 330 Ma (A, B, and C), 230 Ma (D, E, and F), 160 Ma (G, H, and I), and the present day (J, K, and L) for case TG2. See Fig. 2 for plate boundaries and craton symbols.

overall time dependence of dynamic topographies remains similar to that in case TG1 (Fig. 3B and C). Again, the localized plumes show some influences on the time dependent dynamic topography, for example, for the Slave craton at  $\sim 140$  Ma (Fig. 3B) and for the Kaapvaal craton at  $\sim 230$  Ma (Fig. 3C).

## 4. Discussion

### 4.1. The present-day dynamic topography and its magnitude

It is well known that ocean depths for seafloor older than 80 Ma are shallower than predicted from the half-space cooling model — a feature that is sometimes referred to as topographic flattening (e.g., Hillier and Watts, 2005; Parsons and Sclater, 1977). This topographic flattening is prominent in the Pacific and Atlantic, and is sometimes recast as the Pacific and African superswells (Davies and Pribac, 1993; Lithgow-Bertelloni and Silver, 1998; McNutt, 1998; Nyblade and Robinson, 1994). The topographic flattening has been explained in terms of a plate model (Parsons and Sclater, 1977) or inhomogeneous thermal mixing from mantle convection (e.g., Davies, 1999). However, the topographic flattening is not just controlled by seafloor age, and the plate model that has seafloor age as the only controlling parameter leaves significant unexplained residual topography in the mid-Pacific (Zhong et al., 2007). Huang and Zhong (2005) proposed

that trapped heat below the relatively old and thick lithosphere may be the key to explaining the elevated topography at old seafloor.

Our calculations presented here represent the first effort to incorporate the effects of both lithospheric cooling and mantle convection on surface topography in time-dependent mantle convection models. Our models reproduce the first order seafloor topography including the topographic subsidence from mid-ocean ridges to old ocean basins (Fig. 1A) and the reduced topography relative to the half-space cooling model prediction (Fig. 1E). Notice that the observed topography–age relation for the Pacific in Fig. 1E is from Zhong et al. (2007) that removed the effects of sediments, seamounts, and large igneous provinces and was also corrected for the effect of water to be compared with our model topography here. Our dynamic topography calculations using mantle buoyancy below 200 km depth also reproduce the Pacific and African superswells (Fig. 1D) that contribute significantly to the reduced topography relative to the half-space cooling model in these regions (Fig. 1E), and are broadly consistent with previous dynamic topography studies (e.g., Lithgow-Bertelloni and Silver, 1998; Panasyuk and Hager, 2000). In particular, our models show that the Pacific and African superwell topography is related to the dynamically produced superplume structures near the CMB (Fig. 2N) and trapped heat below the lithosphere in these regions (Fig. 2O) (Huang and Zhong, 2005).

However, the amplitude of superwell dynamic topography of  $\sim 400$  m in our model (Fig. 1D) is smaller than the inferred swell

topography of ~1000 m relative to the plate models (e.g., Lithgow-Bertelloni and Silver, 1998; Panasyuk and Hager, 2000). This is also evident in Fig. 1E that the observed topography for the Pacific plate (Zhong et al., 2007) is noticeably shallower at relatively old ages (>100 Ma) than our model prediction (curve A in Fig. 1E). The amplitude of dynamic topography has been debated in geodynamics (e.g., Gurnis, 1990; Le stunff and Ricard, 1997). There are two possible reasons for the discrepancy between our model results and the observed. First, numerical resolution in our models may not be adequate to resolve sub-lithospheric small-scale convection process near the lithosphere–anthenosphere boundary that is known to erode the lithospheric thermal structure to cause reduced topography at relatively old seafloor (e.g., Huang and Zhong, 2005). That the observed topography is deeper than our model prediction between 20 and 80 Ma in Fig. 1E may also reflect inadequate numerical resolution for lithosphere. Second, uncertainties in some of our model parameters may also contribute to the small dynamic topography predictions. Increasing internal heating generation rate may lead to more “trapped” heat or higher temperature in the mantle below old lithosphere that may increase surface dynamic uplift in these regions (Huang and Zhong, 2005). In convection models, if the self-gravitation is ignored, dynamic topography is given as  $h = \sigma_{tr} \alpha \Delta T / Ra$  (Zhong et al., 2008), where  $\sigma_{tr}$  is non-dimensional stresses and the other parameters are listed in Table 1. Even for a fixed Rayleigh number  $Ra$ ,  $h$  depends on the choice of thermal expansion  $\alpha$  and temperature difference across the mantle  $\Delta T$ , both of which have some uncertainties. Also the amplitude of the topography increases with reduced  $Ra$  (i.e., increased reference mantle viscosity) (Lassak et al., 2010). If scaled with parameters in Table 1, the average viscosities for the upper and lower mantles in our models are  $\sim 4.5 \times 10^{19}$  Pa s and  $\sim 7 \times 10^{21}$  Pa s, respectively. However, mantle viscosities may be higher, according to post-glacial rebound studies (e.g., Mitrovica and Forte, 2004; Paulson et al., 2007; Simons and Hager, 1997) and gravity studies (Harig et al., 2010), and this may help reconcile the difference in the amplitude of dynamic topography. We also found that the amplitude of dynamic topography depends weakly on lithospheric viscosity. More studies are needed to further address these issues including the effects of lateral variations in viscosity between sub-continental and sub-oceanic mantles (e.g., Cadec and Fleitout, 2003).

Subduction dip angles are known to affect both the amplitude and wavelength of dynamic topography on the overriding continental plates (e.g., Liu et al., 2008). In our models, plate motions and plate geometries are fixed for each stage that may last between 10 and 50 Ma (Zhang et al., 2010). Without continuously migrating plate boundaries for the overriding plates, subducted slabs may show a stair-step pattern in the mantle and shallow-angle subduction cannot be produced (Bunge and Grand, 2000; Liu et al., 2008). While this needs to be modeled more realistically in the future, we think that the general results of our dynamic topography are robust.

#### 4.2. Continental vertical motion histories and implications for mantle dynamics

A large number of mantle models for dynamic topography have been formulated to understand continental flooding records, the history of sedimentation and erosion as preserved in stratigraphic sequences, patterns of marine incursion, and river drainage reversal (e.g., DiCaprio et al., 2009; Gurnis, 1993; Gurnis et al., 1998; Mitrovica et al., 1989; Moucha et al., 2008; Pysklywec and Mitrovica, 1999; Shephard et al., 2010). Our work is distinct from previous studies in two key ways. First, most past work focused on continental vertical motions associated with evolution of subducting slabs, however, other mantle structures such as broad mantle upwellings (i.e., superplumes) may also exert significant control on continental elevation (e.g., Lithgow-Bertelloni and Silver, 1998). Our models incorporate not only subducted

slabs but also the broad mantle upwellings that are both determined dynamically. Second, we compare the burial and unroofing histories inferred from apatite (U–Th)/He (AHe) and apatite fission-track (AFT) thermochronology studies in several cratonic regions directly with the elevation change histories predicted by our models. Advances in thermochronology methods and rigorous evaluation of the internal consistency of AHe and AFT datasets are shedding new insights into the low temperature histories of cratonic regions (e.g., Flowers, 2009; Flowers and Kelley, 2011), but the potential constraints imposed by these cratonic data on mantle dynamic models have not yet been fully exploited. This approach also differs in comparing the evolution of predicted dynamic topography with burial-unroofing histories over time (Flowers et al., in press), rather than evaluating the consistency of model predictions with thermochronology constraints at particular points in time (e.g., East Africa, Pik et al., 2003; Moucha and Forte, 2011). While the effects of dynamic topography on erosion and sedimentation are likely complicated (e.g., Burgess and Gurnis, 1995), one may reasonably expect that dynamic subsidence may lead to sedimentation or burial at the surface, while uplift may cause erosion or unroofing. The first-order burial and unroofing patterns revealed by the thermochronology datasets are the most robust aspects of the results, with the absolute burial depths of lesser importance for the comparative analysis below. Uncertainties associated with interpretation of the Slave and Kaapvaal craton thermochronology datasets are discussed in detail by Ault et al. (2009), Flowers and Schoene (2010), and Flowers et al. (in press).

We first consider the Slave craton of North America. Our models predict ~1000 m of surface uplift of the Slave craton from 300 to 240 Ma due to warming of the mantle from 330 Ma to 240 Ma below northern Pangea associated with broad mantle upwellings (Figs. 2A, B, and 3B). In some of the models (e.g., TG3) this phase of uplift is preceded by a subsidence episode induced by continuous cooling of the mantle by cold subducted slabs. These results show the influence of both subduction and broad upwellings on continental vertical motions. AHe thermochronology data from the Slave craton demand significant (>4 km) burial of the craton by sedimentary rocks in Paleozoic time, followed by substantial erosion from ~330 to 250 Ma that unroofed the Paleozoic strata (Ault et al., 2009). Flowers et al. (in press) found that this burial-unroofing history is consistent with the mantle dynamic model predictions (Fig. 5A). We more fully explored the range of parameter space for our models in our current study. The Slave craton unroofing phase is synchronous with the dynamic uplift between 330 Ma and 240 Ma predicted by all four models (Figs. 5A and 3B). The pre-330 Ma burial episode in the Slave craton recorded by the thermochronology data is consistent with the dynamic subsidence phase predicted by case TG3 characterized by less subduction before 450 Ma. These results suggest that thermochronology data help constrain dynamic models and that this approach should be further explored in future studies.

We next compare our results for the Kaapvaal craton of southern Africa with geological constraints on the post-300 Ma history of elevation change. The region is last known to have been at sea level during deposition of the Karoo Supergroup from ca. 300–180 Ma, but the timing of elevation gain of the southern African Plateau is controversial. Some have argued for uplift in mid- to Late Tertiary time based largely on correlation of erosion surfaces across the plateau (e.g., Burke and Gunnell, 2008; Partridge and Maud, 1987). In contrast, a variety of thermochronology data that indicate that the majority of unroofing occurred in Mesozoic time has strengthened the case for plateau surface uplift in the Mesozoic (e.g., Brown et al., 2002; Flowers and Schoene, 2010; Tinker et al., 2008) (Fig. 5B).

Fig. 5B compares our predicted vertical motion history for the Kaapvaal craton with the post-300 Ma burial and unroofing history for the eastern craton from Flowers and Schoene (2010). Our dynamic models predict a gradual, nearly monotonic subsidence from 400 to 200 Ma followed by a rapid drop in dynamic topography that ends at ~180 Ma when Pangea starts to break up (Fig. 3C). This is compatible

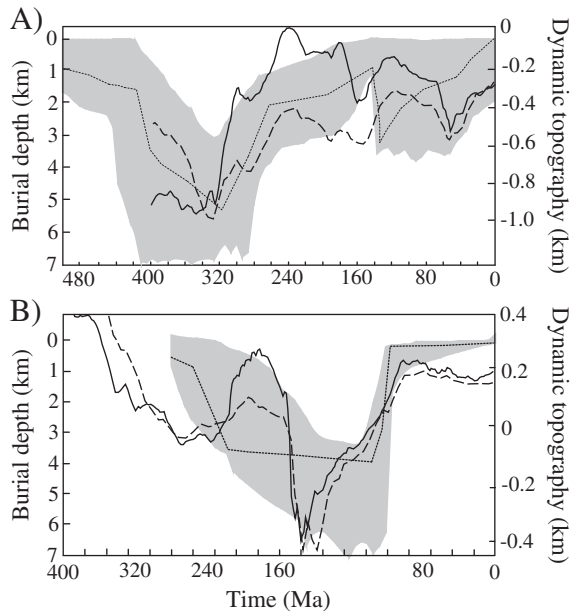


**Fig. 5.** The trend comparisons of dynamic topography histories with the burial-unroofing histories from thermochronology studies for the Slave (A) and Kaapvaal cratons (B). The solid and dashed curves are from cases TG1 and TG3, respectively. The gray shaded domains encompass thermal histories with good fits to the thermochronology data, and converted to burial depths. The results in (A) are similar to those shown in Flowers et al. (in press), with thermal histories from Ault et al. (2009) converted to burial depths assuming a modern day surface temperature of 0 °C and a typical cratonic geothermal gradient of 20 °C/km. The thermal histories inferred by Flowers and Schoene (2010) for the Kaapvaal craton are converted to burial depths in (B) assuming a modern surface temperature of 18 °C and 20 °C/km cratonic geotherm. Refer to those papers for additional discussion regarding the choice of geothermal gradient. Dotted lines are best-fit burial curves.

with the known subsidence of the region during deposition of the Karoo Supergroup. From 180 to ~90 Ma, the craton is predicted to uplift significantly, coincident with unroofing in the ~150 to ~100 Ma time interval indicated by the thermochronology results. Uplift of the southern African Plateau, including the Kaapvaal craton, from 160 Ma to 90 Ma may result from that region moving over the African superplume that develops in our models at that time (Figs. 2 and 3C). Thus the dynamic topography history agrees to first order with the burial-unroofing history from the thermochronology studies (Fig. 5B), suggesting that uplift of the Kaapvaal craton and South Africa occurred in the Mesozoic (Brown et al., 2002; de Wit, 2007; Flowers and Schoene, 2010), rather than in the Cenozoic (Burke, 1996; Burke and Gunnell, 2008). Additional thermochronology studies elsewhere in the plateau are required to more fully test these results.

We briefly compare our model predictions for the Sao Francisco craton of South America and the Yilgarn craton of Australia with thermochronology data from those regions. The predicted vertical motion history for the Sao Francisco craton is similar to that for the Kaapvaal craton because of their proximal locations prior to Gondwana breakup. AFT thermochronology data for the Sao Francisco craton suggest significant unroofing between ~130 and 50 Ma (Harman et al., 1998), broadly overlapping the interval of surface uplift predicted by our models (Fig. 3A). In contrast, however, assessment of Yilgarn craton data reveals that existing AFT data from the northern Yilgarn craton imply long-term continuous cooling and denudation since the end of the Paleozoic (Weber et al., 2005), whereas our model predicts protracted subsidence (Fig. 3A). We reiterate here that this analysis for the Sao Francisco and Yilgarn cratons are first-order comparisons only, and a more comprehensive evaluation of factors contributing to the denudation histories of these regions is required to more fully evaluate these results.

The first-order agreement between predicted elevation change and the burial-unroofing histories for the Kaapvaal and Slave cratons has

important implications for mantle dynamics and evolution of the African superplume. In the general framework of mantle convection and supercontinent cycle proposed by Zhang et al. (2010) and Zhong et al. (2007), the mantle in the African hemisphere, as the destination of subducted slabs, should be relatively cold before and during the early stages of Pangea formation, and the present-day African superplume as observed seismically may not have formed until as recently as ~200 Ma. Slave craton burial before ~330 Ma may reflect cooling of the mantle below Laurussia during Pangea assembly that caused surface subsidence, while unroofing between ~330 and ~250 Ma may have resulted from warming of the mantle after Pangea assembly that generated dynamic uplift (Fig. 2). Kaapvaal craton unroofing from ~150 Ma to 100 Ma is consistent with the uplift during the movement of the African continent over the developing African superplume following Pangea breakup (Fig. 2). Future studies in modeling mantle dynamics and in inferring continental vertical motion histories from geological observations should help further constrain and test our dynamic models for supercontinent cycles and mantle structure evolution, and also test alternative models such as the long-term (~500 Ma) stable African superplume (e.g., Burke et al., 2008; Torsvik et al., 2010).

## 5. Conclusions

We have developed a model for dynamic topography and its history for the last 400 Ma based on a global mantle convection model with imposed surface plate motion history. In particular, we predicted vertical motion histories for four continental cratons, and compared them with the burial-unroofing histories inferred from thermochronology studies. The major findings are summarized as followed:

- 1) The present-day dynamic topography from our models shows topographic highs in the Pacific and African–Atlantic regions that are similar to the Pacific and African superswells in the previously derived residual topography maps, suggesting that the superswells are dynamically supported. The Pacific and African superswells are related to the broad, warm structures (i.e., superplumes) in the deep mantle that help warm the upper mantle below the superswells, particularly in the Pacific.
- 2) The continental vertical motions in our models are affected not only by subduction but also by broad mantle upwellings. The models predict that the Slave craton in North America subsides before Pangea assembly due to subduction that cools the mantle under Laurussia, but the craton uplifts significantly from 330 to 240 Ma, caused by warming of the mantle below Laurussia. The Kaapvaal craton of southern Africa is predicted to undergo mostly subsidence from 400 to ~180 Ma but shows uplift from ~180 to 90 Ma before becoming stable for the last 90 Ma. The vertical motion history for the Sao Francisco craton of South America is similar to that for the Kaapvaal craton, while the Yilgarn craton of Australia shows mostly subsidence for the last 400 Ma.
- 3) The predicted elevation change histories for the Slave and Kaapvaal cratons compare well with the burial-unroofing histories inferred from thermochronology studies, thus to first order supporting our dynamic models including the development of the African superplume mantle structure. Future studies on the elevation change of continental cratons using thermochronology techniques can help further test and constrain mantle dynamic models.

## Acknowledgments

This work was supported by NSF EAR-1015669 and NSF EAR-1135382 to Zhong and NSF EAR-0711451 and NSF EAR-0951518 to Flowers. The authors wish to thank constructive reviews by Yanick Ricard as editor, Laurent Husson, and two anonymous reviewers. The CIG is thanked for distributing the software CitcomS that is used in this study.

## References

- Ault, A.K., Flowers, R.M., Bowring, S.A., 2009. Phanerozoic burial and unroofing history of the western Slave craton and Wopmay orogen from apatite (U–Th)/He thermochronometry. *Earth Planet. Sci. Lett.* 284, 1–11.
- Brown, R.W., Summerfield, M.A., Gleadow, A.J.W., 2002. Denudational history along a transect across the Drakensberg Escarpment of southern Africa derived from apatite fission track thermochronology. *J. Geophys. Res.* 107, 2350. doi:10.1029/2001JB000745.
- Bull, A.L., McNamara, A.K., Ritsema, J., 2009. Synthetic tomography of plume clusters and thermochemical piles. *Earth Planet. Sci. Lett.* 278, 152–162.
- Bunge, H.-P., Grand, S., 2000. Mesozoic plate-motion history below the northeast Pacific Ocean from seismic images of the subducted Farallon slab. *Nature* 405, 337–340.
- Bunge, H.-P., Richards, M.A., Lithgow-Bertelloni, C., Baumgardner, J.R., Grand, S., Romanowicz, B., 1998. Time scales and heterogeneous structure in geodynamic earth models. *Science* 280, 91–95.
- Burgess, P.M., Gurnis, M., 1995. Mechanisms for the formation of cratonic stratigraphic sequences. *Earth Planet. Sci. Lett.* 136, 647–663.
- Burke, K., 1996. The African Plateau. *S. Afr. J. Geol.* 99, 341–409.
- Burke, K., Gunnell, Y., 2008. The African erosion surface: a continental-scale synthesis of geomorphology, tectonics, and environmental change over the past 180 million years. *Geol. Soc. Am. Mem.* 201, 66.
- Burke, K., Steinberger, B., Torsvik, T.H., Smethurst, M.A., 2008. Plume generation zones at the margins of Large Low Shear Velocity Provinces on the core–mantle boundary. *Earth Planet. Sci. Lett.* 265, 49–60.
- Cadek, O., Fleitout, L., 2003. Effect of lateral viscosity variations in the top 300 km on the geoid and dynamic topography. *Geophys. J. Int.* 152, 566–580.
- Cazenave, A., Souriau, A., Dominh, K., 1989. Global coupling of Earth surface topography with hotspots, geoid and mantle heterogeneities. *Nature* 340, 54–57.
- Christensen, U.R., 1984. Convection with pressure and temperature dependent non-Newtonian rheology. *Geophys. J. R. Astron. Soc.* 77, 242–284.
- Conrad, C.P., Lithgow-Bertelloni, C., Loudon, K.E., 2004. Iceland, the Farallon slab, and dynamic topography of the North Atlantic. *Geology* 32, 177–180.
- Davies, G.F., 1989. Mantle convection model with a dynamic plate: topography, heat flow, and gravity anomalies. *Geophys. J. Int.* 98, 461–464.
- Davies, G.F., 1999. *Dynamic Earth: Plates, Plumes and Mantle Convection*, 470. Cambridge University Press.
- Davies, G.F., Pribac, F., 1993. Mesozoic seafloor subsidence and the Darwin Rise, past and present. In: Pringle, S., et al. (Ed.), *The Mesozoic Pacific: Geology, Tectonics, and Volcanism*, Geophys. Mono., 77. AGU, Washington, D.C., pp. 39–52.
- de Wit, M.J., 2007. The Kalahari epeirogeny and climate change: differentiating cause and effect from core to space. *S. Afr. J. Geol.* 110, 367–392. doi:10.2113/gssajg.110.2-3.367.
- DiCaprio, L., Müller, R.D., Gurnis, M., Goncharov, A., 2009. Linking active margin dynamics to overriding plate deformation: synthesizing geophysical images with geological data from the Norfolk Basin. *Geochem. Geophys. Geosyst.* 10, Q01004. doi:10.1029/2008GC002222.
- Flowers, R.M., 2009. Exploiting radiation damage control on apatite (U–Th)/He dates in cratonic regions. *Earth Planet. Sci. Lett.* 277, 148–155.
- Flowers, R.M., Kelley, S.A., 2011. Interpreting data dispersion and inverted dates in apatite (U–Th)/He and fission-track datasets: an example from the U.S. midcontinent. *Geochim. Cosmochim. Acta* 75, 5169–5186.
- Flowers, R.M., Schoene, B., 2010. (U–Th)/He thermochronometry constraints on unroofing of the eastern Kaapvaal craton and significance for uplift of the southern African Plateau. *Geology* 38, 827–830.
- Flowers, R.M., Ault, A.K., Kelley, S.A., Zhang, N., Zhong, S.J., in press. Epeirogeny or Eustasy? Paleozoic–Mesozoic vertical motion of the North American continental interior from thermochronometry and implications for mantle dynamics. doi:10.1016/j.epsl.2011.11.015
- Ghosh, A., Becker, T.W., Zhong, S.J., 2010. Effects of lateral viscosity variations on the geoid. *Geophys. Res. Lett.* 37, L01301. doi:10.1029/2009GL040426, 2010.
- Gurnis, M., 1990. Bounds on global dynamic topography from Phanerozoic flooding of continental platforms. *Nature* 344, 754–756.
- Gurnis, M., 1993. Phanerozoic marine inundation of continents driven by dynamic topography above subducting slabs. *Nature* 364, 589–593.
- Gurnis, M., Muller, R., Moresi, L., 1998. Cretaceous vertical motion of Australia and the Australian Antarctic discordance. *Science* 279, 1499–1504.
- Hager, B.H., Richards, M.A., 1989. Long-wavelength variations in the Earth's geoid: physical models and dynamic implications. *Philos. Trans. R. Soc. London, Ser. A* 328, 309–327.
- Harig, C., Zhong, S.J., Simons, F.J., 2010. Constraints on upper-mantle viscosity inferred from the flow-induced pressure gradient across a continental keel. *Geochem. Geophys. Geosyst.* 11, Q06004. doi:10.1029/2010GC003038.
- Harman, R., Gallagher, K., Brown, R., Raza, A., Bizzi, L., 1998. Accelerated denudation and tectonic/geomorphic reactivation of the cratons of northeastern Brazil during the Late Cretaceous. *J. Geophys. Res.* 103, 27,091–27,105.
- Hillier, J.K., Watts, A.B., 2005. Relationship between depth and age in the North Pacific Ocean. *J. Geophys. Res.* 110, B02405. doi:10.1029/2004JB003406.
- Huang, J.S., Zhong, S.J., 2005. Sublithospheric small-scale convection and its implications for residual topography at old ocean basins and the plate model. *J. Geophys. Res.* 110, B05404. doi:10.1029/2004JB003153.
- Karato, S.I., Jung, H., 2003. Effects of pressure on high-temperature dislocation creep in olivine. *Philos. Mag.* 83 (3), 401–414.
- King, S.D., Lowman, J.P., Gable, C.W., 2002. Episodic tectonic plate reorganizations driven by mantle convection. *Earth Planet. Sci. Lett.* 203, 83–91.
- Lassak, T.M., McNamara, A.K., Garner, E.J., Zhong, S.J., 2010. Core–mantle boundary topography as a possible constraint on lower mantle chemistry and dynamics. *Earth Planet. Sci. Lett.* 289, 232–241. doi:10.1016/j.epsl.2009.11.012.
- Le stunff, Y., Ricard, Y., 1997. Partial advection of equi-density surfaces: a solution for the dynamic topography problem? *J. Geophys. Res.* 102, 24655–24667.
- Leng, W., Zhong, S.J., 2008. Controls on plume heat flux and plume excess temperature. *J. Geophys. Res.* 113, B04408. doi:10.1029/2007JB005155.
- Lithgow-Bertelloni, C., Gurnis, M., 1997. Cenozoic subsidence and uplift of continents from time-varying dynamic topography. *Geology* 25, 735–738.
- Lithgow-Bertelloni, C., Richards, M.A., 1998. Dynamics of Cenozoic and Mesozoic plate motions. *Rev. Geophys.* 36, 27–78.
- Lithgow-Bertelloni, C., Silver, P.G., 1998. Dynamic topography, plate driving forces and the African Superswell. *Nature* 395, 269–272.
- Liu, L.J., Spasojevic, S., Gurnis, M., 2008. Reconstructing Farallon Plate subduction beneath North America back to the Late Cretaceous. *Science* 322, 934–938.
- McNamara, A.K., Zhong, S.J., 2005. Thermochemical structures beneath Africa and the Pacific Ocean. *Nature* 437, 1136–1139.
- McNutt, M.K., 1998. Superswell. *Rev. Geophys.* 36, 211–244.
- Mitrovica, J.X., Forte, A.M., 2004. A new inference of mantle viscosity based upon joint inversion of convection and glacial isostatic adjustment data. *Earth Planet. Sci. Lett.* 225, 177–189.
- Mitrovica, J., Beaumont, C., Jarvis, G., 1989. Tilting of continental interiors by the dynamical effects of subduction. *Tectonics* 8, 1079–1094.
- Moucha, R., Forte, A.M., 2011. Changes in African topography driven by mantle convection. *Nat. Geosci.* doi:10.1038/NGEO1235
- Moucha, R., Forte, A.M., Rowley, D.B., Mitrovica, J.X., Simmons, N.A., Grand, S.P., 2008. Mantle convection and the recent evolution of the Colorado Plateau and the Rio Grande Rift valley. *Geology* 36, 439–442.
- Nyblade, A.A., Robinson, S.W., 1994. The African superswell. *Geophys. Res. Lett.* 21, 765–768. doi:10.1029/94GL00631.
- Panasuyuk, S., Hager, B.H., 2000. Models of isostatic and dynamic topography, geoid anomalies, and their uncertainties. *J. Geophys. Res.* 105. doi:10.1029/2000JB900249.
- Parsons, B., Sclater, J.G., 1977. An analysis of the variation of ocean floor bathymetry and heat flow with age. *J. Geophys. Res.* 82, 803–827.
- Partridge, T.C., Maud, R.R., 1987. Geomorphic evolution of southern Africa since the Mesozoic. *S. Afr. J. Geol.* 90, 179–208.
- Paulson, A., Zhong, S.J., Wahr, J., 2007. Inference of mantle viscosity from GRACE and relative sea level data. *Geophys. J. Int.* 171, 497–508.
- Pik, R., Marty, B., Carignan, J., Lave, J., 2003. Stability of the upper Nile drainage network (Ethiopia) deduced from (U–Th)/He thermochronometry: implications for uplift and erosion of the Afar plume dome. *Earth Planet. Sci. Lett.* 215, 73–88.
- Pysklywec, R., Mitrovica, J.X., 1999. The role of subduction-induced subsidence in the evolution of the Karoo Basin. *J. Geology* 107, 155–164.
- Ricard, Y., Richards, M.A., Lithgow-Bertelloni, C., Lestunff, Y., 1993. A geodynamic model of mantle mass heterogeneities. *J. Geophys. Res.* 98, 21,895–21,909.
- Scotese, C.R., 2001. *Atlas of Earth history*. PALEOMAP Progress Report 90–0497. Dept. of Geol., Univ. of Tex. at Arlington, Texas.
- Shephard, G.E., Müller, R.D., Liu, L.J., Gurnis, M., 2010. Miocene drainage reversal of the Amazon River driven by plate–mantle interaction. *Nat. Geosci.* 3, 870–875.
- Simons, M., Hager, B.H., 1997. Localization of the gravity field and the signature of glacial rebound. *Nature* 390, 500–504.
- Spasojević, S., Liu, L.J., Gurnis, M., 2009. Adjoint models of mantle convection with seismic, plate motion and stratigraphic constraints: North America since the Late Cretaceous. *Geochem. Geophys. Geosyst.* 10 (Q05W02). doi:10.1029/2008GC002345.
- Tinker, J., de Wit, M., Brown, R.W., 2008. Mesozoic exhumation of the southern Cape, South Africa, quantified using apatite fission track thermochronology. *Tectonophysics* 455, 77–93. doi:10.1016/j.tecto.2007.10.009.
- Torsvik, T.H., Burke, K., Steinberger, B., Webb, S.J., Ashwal, L.D., 2010. Diamonds sampled by plumes from the core–mantle boundary. *Nature* 466, 352–355.
- van Hunen, J., Zhong, S.J., Shapiro, N.M., Ritzwoller, M.H., 2005. New evidence for dislocation creep from 3-D geodynamic modeling of the Pacific upper mantle structure. *Earth Planet. Sci. Lett.* 238, 146–155.
- Ward, P.L., 1995. Subduction cycles under western North America during the Mesozoic and Cenozoic eras. *Geol. Soc. Am. Spec. Pap.* 299, 12.
- Weber, U.D., Kohn, B.P., Gleadow, A.J.W., Nelson, D.R., 2005. Low temperature Phanerozoic history of the Northern Yilgarn Craton, Western Australia. *Tectonophysics* 400, 127–151.
- Wen, L., Anderson, D.L., 1997. Layered mantle convection: a model for geoid and topography. *Earth Planet. Sci. Lett.* 146, 367–377.
- Zhang, N., Zhong, S.J., 2011. Heat fluxes at the Earth's surface and core–mantle boundary since Pangea formation and their implications for the geomagnetic superchrons. *Earth Planet. Sci. Lett.* doi:10.1016/j.epsl.2011.04.001.
- Zhang, N., Zhong, S.J., Leng, W., Li, Z.X., 2010. A model for the evolution of the Earth's mantle structure since the Early Paleozoic. *J. Geophys. Res.* 115, B06401. doi:10.1029/2009JB006896.
- Zhong, S.J., Davies, G.F., 1999. Effects of plate and slab viscosities on geoid. *Earth Planet. Sci. Lett.* 170, 487–496.
- Zhong, S.J., Watts, A.B., 2002. Constraints on the dynamics of mantle plumes from uplift of Hawaiian islands. *Earth Planet. Sci. Lett.* 203, 105–116.
- Zhong, S.J., Zuber, M.T., Moresi, L.N., Gurnis, M., 2000. Role of temperature dependent viscosity and surface plates in spherical shell models of mantle convection. *J. Geophys. Res.* 105, 11063–11082.
- Zhong, S.J., Ritzwoller, M., Shapiro, N., Landuyt, W., Huang, J.S., Wessel, P., 2007. Bathymetry of the Pacific Plate and its implications for thermal evolution of lithosphere and mantle dynamics. *J. Geophys. Res.* 112, B06412. doi:10.1029/2006JB004628.
- Zhong, S.J., McNamara, A.K., Tan, E., Moresi, L., Gurnis, M., 2008. A benchmark study on mantle convection in a 3-D spherical shell using CitcomS. *Geochem. Geophys. Geosyst.* 9, Q10017. doi:10.1029/2008GC002048.